NANO LETTERS

pubs.acs.org/NanoLett Letter

# Reconfigurable Pinwheel Artificial-Spin-Ice and Superconductor Hybrid Device

Yang-Yang Lyu,[+] Xiaoyu Ma,[+] Jing Xu, Yong-Lei Wang,* Zhi-Li Xiao,* Sining Dong, Boldizsar Janko, Huabing Wang,* Ralu Divan, John E. Pearson, Peiheng Wu, and Wai-Kwong Kwok

Cite This: *Nano Lett.* 2020, 20, 8933−8939 Read Online

ACCESS | Metrics & More | Article Recommendations | Supporting Information

**ABSTRACT:** The ability to control the potential landscape in a medium of interacting particles could lead to intriguing collective behavior and innovative functionalities. Here, we utilize spatially reconfigurable magnetic potentials of a pinwheel artificial-spin-ice (ASI) structure to tailor the motion of superconducting vortices. The reconstituted chain structures of the magnetic charges in the pinwheel ASI and the strong interaction between magnetic charges and superconducting vortices allow significant modification of the transport properties of the underlying superconducting thin film, resulting in a reprogrammable resistance state that enables a reversible and switchable vortex Hall effect. Our results highlight an effective and simple method of using ASI as an in situ reconfigurable nanoscale energy landscape to design reprogrammable superconducting electronics, which could also be applied to the in situ control of properties and functionalities in other magnetic particle systems, such as magnetic skyrmions.

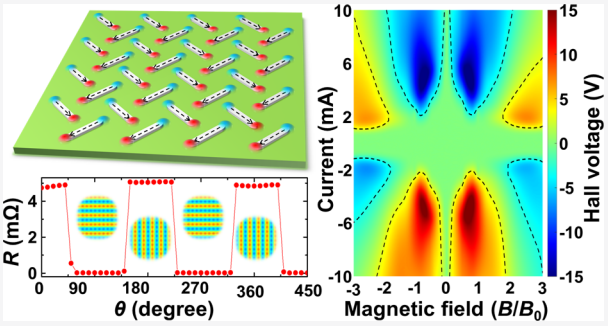


**KEYWORDS:** *Artificial spin ice, Superconducting vortex, Hybrid device, Vortex Hall effect*

Abrikosov vortices are quantized magnetic flux in a type II superconductor, having nonsuperconducting cores surrounded by swirling supercurrents.[1] As moving vortices dissipate energy, controlling the motion of vortices is essential to tailor superconducting electromagnetic properties for designing innovative electronics,[2] such as vortex pumps, diodes, lenses, and rectifiers.[3] Vortex dynamics is an active research area, with respect to both fundamental physical studies of vortex matter and practical electronic and power applications.[4] Vortices can be trapped by nanoscale defects introduced by ion irradiation,[5,6] grain boundaries,[7,8] nanostrained regions,[9] and patterned nanostructures via advanced nanofabrication.[10−16] However, in the aforementioned approach, the spatial vortex pinning potential landscapes produced by defects are fixed, once the samples are synthesized. In contrast, superconducting vortices can also interact with magnetic nanostructures.[17−27] The controlled magnetization of magnetic nanostructures with an applied magnetic field allows in situ tuning of the vortex pinning potential, enabling reconfigurable superconducting functionalities.[25−27] Recently, a particular type of magnetic nanostructure, called artificial spin ice (ASI), was used as nanoscale reconfigurable magnetic landscapes to modulate the behavior of vortices in a hybrid ferromagnetic/superconducting structure.[28,29] The highly tunable and wide spectrum of magnetic configurations of ASI structures allow the tuning of vortex motion and superconducting transport properties in a more flexible way. For example, a reprogrammable vortex diode has been recently realized by patterning a triaxial ASI on top of a superconducting film,[29] and a reversible vortex ratchet effect was demonstrated by using an artificial kagome spin ice.[28] Here, we present a new ASI and superconductor heterostructure consisting of a pinwheel (or chiral) ASI array on top of a superconducting film (Figure 1a). The switchable chainlike magnetic charges in the pinwheel ASI lead to a strong modulation of vortex motion, allowing us to achieve switching of energy dissipation and reversal of the vortex Hall effect.

ASIs contain arrays of interacting single domain nanoscale bar magnets.[30] They were introduced to investigate complex magnetic phenomena, such as geometric frustration. There are various types of ASIs, each containing nanomagnets of different arrangements and exhibiting unique properties.[31] Recently, a pinwheel ASI was created by rotating each of the magnetic nanobars in a square ASI by 45°, forming an array of orthogonally oriented nanomagnets pointed toward the midpoint of each other.[32,33] The pinwheel ASI forms a 4-fold degenerate ferromagnetic order with easily tunable

**Received:** October 13, 2020
**Revised:** November 23, 2020
**Published:** November 30, 2020

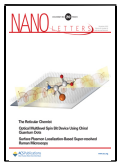

Downloaded from pubs.acs.org/nalefd/article-pdf/20/12/8933/17691840/nl0c04093.pdf by NANJING UNIV user on 24 August 2026

ACS Publications © 2020 American Chemical Society



https://dx.doi.org/10.1021/acs.nanolett.0c04093
*Nano Lett.* 2020, 20, 8933−8939

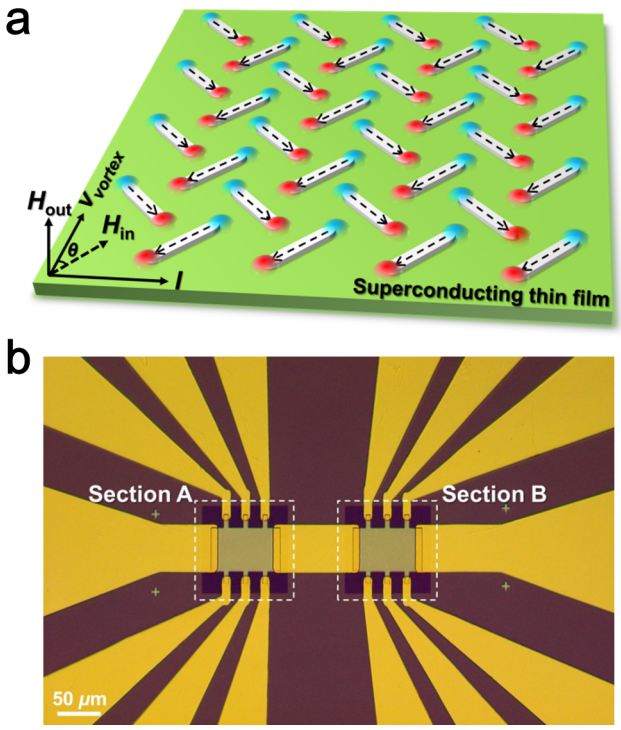


**Figure 1.** Hybrid device of pinwheel ASI and superconductor. (a) Schematic diagram of the hybrid system consisting of a pinwheel ASI structure on top of a superconducting film. The arrows in the left lower corner indicate the directions of the applied current, vortex motion, and external out-of-plane and in-plane magnetic fields. The dashed arrows on the magnetic nanobars represent the magnetization directions, and the red and blue spots indicate positive and negative magnetic charges, respectively. (b) Optical image of the heterostructure sample on a $Si/SiO_2$ substrate. The yellow area is covered by a 100 nm thick layer of gold. The gray rectangles and dark squares show the MoGe microbridges and areas covered by the ASI arrays, respectively. Additional data on sections A and B including images of the nanomagnets and the magnetic charges as well as the results of transport measurements are presented in Figures 2 and 3, respectively.

magnetic configurations via an in-plane external magnetic field.[33] The interaction between a nanomagnet in an ASI and a vortex in a superconductor can be viewed as a dumbbell of magnetic charges "one negative, one positive" attracting and/or repelling a superconducting vortex, respectively.[29] As shown in Figure 1a, one unique feature of pinwheel ASI is the formation of alternating rows of positive and negative magnetic charge chains, creating alternating negative (low) potential valleys and positive (high) potential ridges for superconducting vortices. The orientation of these charge chains can be conveniently rotated 90° by tuning the ASI's magnetization with an in-plane magnetic field (Figure 2b,e). This leads to a reconfigurable magnetic potential landscape, enabling the control of vortex motion to realize a reversible superconducting switch and a programmable vortex Hall effect. Our results could stimulate future investigations to explore abilities and advantages of reprogrammable hybrid devices based on reconfigurable magnetic potentials.

Our experiments were carried out on a heterostructure containing a pinwheel ASI array fabricated on top of a 100 nm thick superconducting $Mo_{0.79}Ge_{0.21}$ (MoGe) film (Figure 1a). An image of the sample is shown in Figure 1b. The superconducting MoGe film was patterned into a microbridge containing two separate sections (for demonstrating different effects) using photolithography. Subsequently, two pinwheel ASI arrays, oriented 45° from each other were separately fabricated on top of the MoGe sections via e-beam lithography, followed with e-beam evaporation of permalloy. The permalloy islands have dimensions of 350 nm ($l$) × 80 nm ($w$) × 25 nm ($d$). In each section there are 18 000 nanomagnets at the measured area. Lastly, 100 nm thick gold electrodes were deposited for measuring both regular (longitudinal) and Hall (transverse) voltages. Transport measurements were conducted in a three-axis superconducting vector magnet, which provides magnetic fields in any desired 3D orientation. The applied current is directed along the length of the microbridge. An oriented in-plane magnetic field (Figure 1a) is used to tailor the magnetic charge configurations of the ASI and is turned off when the transport measurements are being conducted. During the transport measurements an out-of-plane magnetic field (perpendicular to the sample plane) is applied to tune the density of superconducting vortices in the MoGe film (Figure 1a). The superconducting transition temperature $T_c$ of our MoGe film is 6.9 K. The experiments were carried out at a temperature of 6 K. Additional sample fabrication and experimental details can be found in ref 29.

The pinwheel ASI array of section A of the sample is shown in Figure 2a along with the applied current and vortex motion directions. The magnetic charge order can be in situ switched between vertical charge chains and horizontal charge chains, as shown by the magnetic force microscopy images in Figure 2b,e, respectively. The current induced Lorentz force on the vortices is perpendicular to the applied current (Figure 2a). In Figure 2c,f, respectively, we show the magnetic field and current dependences of the measured voltages under the vertical and horizontal magnetic chains. The magnetic field is normalized to the first matching field, $B_0$ = 165.6 Oe, where the density of vortices is equivalent to the density of nanomagnets (detailed calculation of $B_0$ can be found in the supplemental document). That is, at $B = B_0$ the number of superconducting vortices is the same as that of the nanomagnets. The black dashed lines in Figure 2c,f highlight the critical current ($I_c$) curves defined by voltage criteria of ±1 μV. We can see a clear difference of current−voltage ($I$−$V$) characteristics obtained when the magnetic charge chains are vertical and horizontal, respectively, indicating distinct vortex motion behaviors.

For a direct comparison, we extract the critical current curves from Figure 2c,f, and plot them in the same graph (Figure 2d). In both cases, the $I_c(B)$ curves show clear peaks/kinks at the magnetic fields of $B_0$ and $0.5B_0$. These are typical features of vortex-matching effects induced by dynamical matching of an ordered vortex lattice to the regularly distributed pinning potentials.[13−29] To unveil the microscopic distribution and dynamics of the vortices, we conduct molecular dynamics (MD) simulations (details on the method are described in ref 29). The simulations (Figure S1) show ordered vortices at the magnetic fields of $B_0$ and $0.5B_0$. Figure 2d shows that at $B < B_0$ the critical currents are enhanced when the orientation of the magnetic charge chains is switched from vertical to horizontal. This indicates that vortex motion is hindered under the potentials created by the horizontal charge chains. As mentioned earlier, the chainlike magnetic charges produce alternating low potential valleys and high potential ridges. Our MD simulations (Video S1) clearly show that vortices move along low-potential valleys induced by the vertical magnetic charge chains, while they are hindered or

Downloaded from pubs.acs.org/nanolett/article-pdf/20/12/8933/17691840/nl0c04093.pdf by NANJING UNIV user on 24 August 2026


https://dx.doi.org/10.1021/acs.nanolett.0c04093
Nano Lett. 2020, 20, 8933−8939

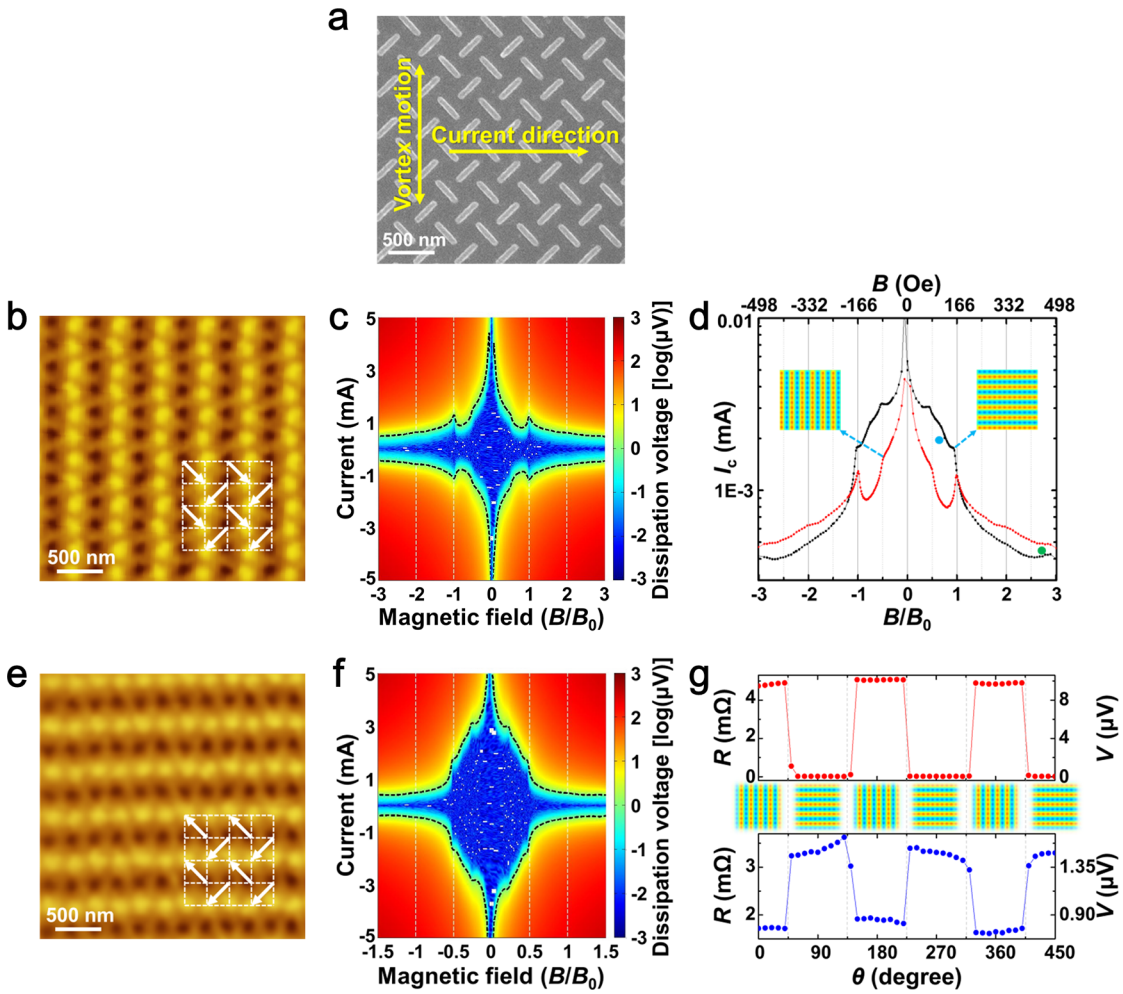


**Figure 2.** Reversible superconducting switch. (a) Scanning electron microscopy image of the pinwheel ASI in section A in Figure 1b. (b) and (e) Magnetic force microscopy images of the vertical and horizontal chains of magnetic charges from the pinwheel ASI shown in (a). The bright and dark spots are positive and negative magnetic charges, respectively. The white arrows represent magnetization directions of the nanomagnets. (c) and (f) Magnetic field and current dependences of the longitudinal voltages corresponding to the magnetic charge configurations shown in (b) and (e), respectively. The color scale is for the values of the log $|V|$. The black dashed lines indicate the critical currents defined by a voltage criterion of $\pm 1\ \mu$V. The magnetic field is in unit of $B_0$ = 165.6 Oe, corresponding to one vortex per nanomagnet. (d) Magnetic field dependence of the critical current $I_c(B)$ curves extracted from (c) and (f). (g) Reversible switching of the resistance states. Results shown in the top and bottom graphs in (g) were obtained at $I$ = 2 mA, $B$ = 120 Oe and $I$ = 0.45 mA, $B$ = 450 Oe, as marked in (d) by the blue and green points, respectively. The angle $\theta$ corresponds to the orientation of the in-plane magnetic field used to polarize the ASI array (see Figure 1). The corresponding magnetic charge configurations are shown in the middle panel.

even arrested when the magnetic charge chains are horizontal. This is because along the low-potential valleys (quasi-1D) of the vertical charge-ordered structure, the pinning potential is much flatter than that across the alternating low-potential valleys and high potential ridges of the horizontal charge-ordered structure. Therefore, the vertical magnetic charge chains produce easy vortex flow channels, and the horizontal charge chains create large potential barriers that prevent vortex motion. This leads to very large critical currents when the charge chains are horizontal, as compared to the ones induced by the vertical magnetic charge chains.

The switchable and rotatable magnetic charge chains of the pinwheel ASI provide us with a convenient way to in situ switch on/off the motion of vortices, enabling a superconducting switch for vortex flow. We demonstrate the superconducting vortex-flow switch by alternately toggling the ASI's magnetization states between vertical and horizontal charge chains (Figure 2g). To realize such a switch, we bias the current and the magnetic field (out-of-plane) to the values marked by the blue point in Figure 2d. At this point, the value of the measurement current lies in between the high and low critical currents of the horizontal and vertical charge chains, respectively. In this case, we can switch the sample between dissipationless state and vortex flow (resistive) state by toggling the ASI's magnetic charge order by simply rotating the in-plane magnetic field. The top portion of Figure 2g shows the switching on and off of the dissipationless states. From Figure 2d, we also see that the two critical current curves cross at $B = B_0$, leading to a reversal of the critical currents under the vertical and horizontal charge chains at $B > B_0$. At $B = B_0$, the number of vortices equals that of the nanomagnets, so all the vortices are trapped by the attractive magnetic charges. Additional vortices generated at $B > B_0$ are located at interstitial sites. In this case, the vortex−vortex interaction plays an important role. As shown in Video S2, under vertical magnetic charge chains, all the interstitial vortices are


https://dx.doi.org/10.1021/acs.nanolett.0c04093
Nano Lett. 2020, 20, 8933−8939

Downloaded from pubs.acs.org/nalefd/article-pdf/20/12/8933/1769184O/nl0c04093.pdf by NANJING UNIV user on 24 August 2026

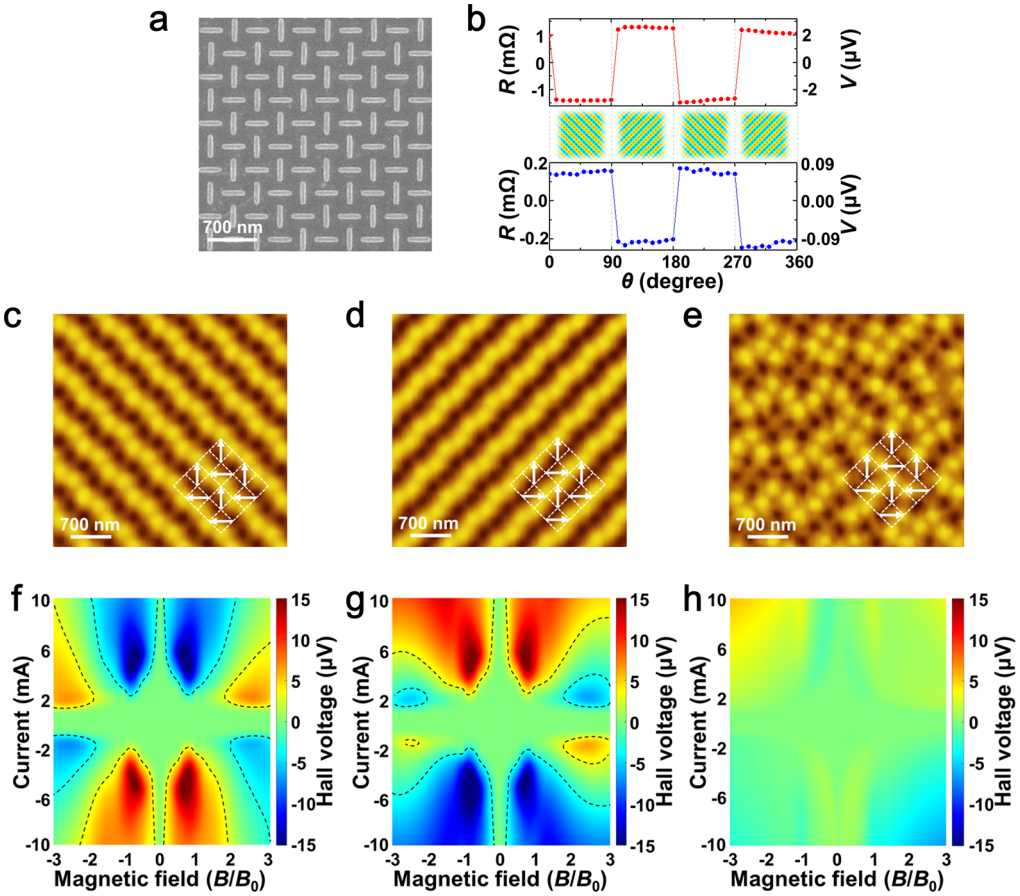


**Figure 3.** Reprogrammable vortex Hall effect. (a) Scanning electron microscopy image of the pinwheel ASI in section B in Figure 1b. (b) Reversible switching of the vortex Hall voltages at low magnetic field (120 Oe) (top graph) and at high magnetic field (400 Oe) (bottom graph). (c−e) Magnetic force microscopy images of the −45° and +45° magnetic charge chains and a random configuration of magnetic charges obtained from (a). (f−h) Magnetic field and current dependences of the vortex Hall voltage respectively, obtained under the magnetic charge configurations shown in (c−e).

immobilized and pinned by neighboring trapped vortices and the repulsive magnetic charges. In contrast, under horizontal charge chains, lines of interstitial vortices first move together horizontally to seek gaps between the peaks (or repulsive charges) in the high potential ridges and then pass the high potential ridges by squeezing along the gaps, resulting in a much lower critical current. This results in a reversal of the critical current behavior for the two ASI's configurations at low and high magnetic fields. By biasing a current between the two critical current curves at $B > B_0$ (the green point in Figure 2d), we could reverse the polarity of the vortex switch as compared to $B < B_0$ (see the bottom graph of Figure 2g). That is, we can achieve a reconfigurable superconducting vortex-flow switch in which the sequence of the low- and high-resistance states can be reversed by setting the out-of-plane magnetic field from $B < B_0$ to $B > B_0$.

In addition to switching on/off of the vortex motion, the alternating row-by-row attractive potential valleys and repulsive potential ridges provide a perfect system for guided vortex motion. Since vortices are favored to move along the attractive potential valleys, we can tailor the path of moving vortices to deviate from their nominal direction of the Lorentz driven force. For example, we could design a vortex Hall device in which vortices could have a longitudinal component of the motion under a transverse driving force. To demonstrate this, we fabricate a pinwheel ASI array rotated by 45° in section B of the sample (Figures 1b and 3a). Such a pinwheel ASI array produces diagonally oriented magnetic charge chains whose orientation can be in situ switched between −45° (Figure 3c) and +45° (Figure 3d). Since the motion of vortices induces a voltage perpendicular to their moving direction, a longitudinal vortex motion results in a transverse (Hall) voltage. This allows us to detect the vortex Hall effect using the same conventional six-probe electrical contact configuration as that used for investigating the electric charge Hall effect (Figure 1b).

We measured the magnetic field (out-of-plane) and current dependences of the Hall voltages at −45° and +45° orientations of ASI's charge chains. The results are shown in Figure 3f,g, respectively. Clear Hall voltage signals are observed, indicating the realization of the vortex Hall effect. The Hall signal (Figure 3f,g) shows interesting behavior with positive and negative Hall voltage values over the magnetic field and current maps. To further look into the origins of these Hall signals, we carried out MD simulations. Video S3 shows that the vortices move diagonally along the attractive charge order chains (potential valleys) for $B \leq B_0$, where the density of vortices is smaller than that of the attractive charges or nanomagnets. Figure 4a,b shows screenshots of Video S3 (respectively corresponding to the case for −45° and +45° magnetic chains), which show trajectories of the vortex motion. We explain the diagonal vortex motion by drawing


https://dx.doi.org/10.1021/acs.nanolett.0c04093
Nano Lett. 2020, 20, 8933−8939

Downloaded from pubs.acs.org/nanolett/article-pdf/20/12/8933/17691840/nl0c04093.pdf by NANJING UNIV user on 24 August 2026

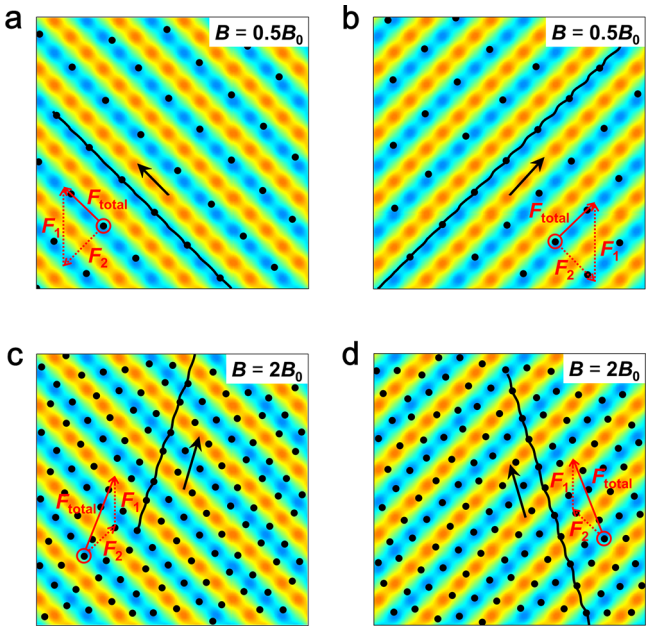


**Figure 4.** Molecular dynamics simulations of the vortex Hall effect. (a−d) Screen shots of simulated vortex motions (from Videos S3 and S4) under $B = 0.5B_0$ (a and b) and $B = 2B_0$ (c and d) for −45°- and 45°-oriented magnetic charge chains. Black dots represent vortices. Blue and red represent attractive and repulsive potentials, respectively. In each figure, the black line is the trajectory for one vortex and the black arrow shows the direction of motion. $F_1$ is the Lorentz driving force induced by the applied current. $F_2$ is the force from magnetic charges. $F_{total}$ is the total force.

the forces on them, as shown in Figure 4a,b. The Lorentz force $F_1$, generated by horizontal electrical currents, is in the vertical direction, and the magnetic charge chains produce force $F_2$ with the direction perpendicular to the chains, preventing vortices from moving across the chains. The resultant force, $F_1 + F_2$, drives the vortices in a diagonal direction, which results in a horizontal vortex velocity, leading to a measurable Hall voltage signal. In Figure 4 and Video S3, we can see that the horizontal components of the vortex motion are in the opposite directions for the case of −45° and +45° magnetic charge chains, resulting in inverted polarities of the Hall signals (Figure 3f,g). Since the corresponding transverse components of vortex velocities are equivalent under both ±45° magnetic charge chain configurations, the longitudinal voltages are identical for the two cases (see Figure S2). In the top graph of Figure 3b, we also demonstrate the switching of Hall signal polarity by rotating the in-plane fields to change the orientation of the magnetic charge chains.

Besides reversing Hall signals by tuning ASI's states, the Hall signals can also be reversed by changing the out-of-plane magnetic field. In Figure 3f,g, the sign of the Hall voltage inverts at high magnetic fields as compared to low magnetic fields. This is again attributed to the strong vortex−vortex interactions. Our simulations for high fields (Figure 4c,d and Video S4) clearly demonstrate that the horizontal component of vortex motion is in the opposite direction as compared to that at low magnetic fields ($B < B_0$) (Figure 4a,b and Video S3). The bottom and top graphs of Figure 3b clearly demonstrate a reversal of the polarity of the Hall switching voltage at different magnetic fields. The reversal of the Hall signal with increasing magnetic fields cannot occur for electronic charges, such as electrons or holes and is a unique property of superconducting vortices.

However, similar to the Hall effect arising from electronic charges, the polarity of the vortex Hall voltage signal is also reversed when the current direction is inverted. This is because an inverted current changes the Lorentz force direction, pushing vortices to move in the opposite direction. However, the Hall voltage signal shows a mirror symmetry with respect to the zero magnetic field line, in contrast to the Hall effect from electronic charges, which shows a reversed Hall voltage when the magnetic field is reversed. For superconducting vortices, reversing the magnetic field would flip their polarity and the Lorenz force acting on them, causing the vortices to move in the opposite direction along the chains. Thus, reversal of the magnetic field orientation will not change the polarity of the Hall voltage signal, giving rise to the mirror symmetry with respect to the zero magnetic field line in Figure 3f,g. Furthermore, the pinwheel ASI can be converted into a random magnetic configuration (Figure 3e), thereby switching off the vortex Hall effect (Figure 3h). This demonstrates another advantage of our ASI and superconductor hybrid device, where the Hall effect can be not only reversed but also switched on and off by tuning the ASI's magnetization state.

The pinwheel (or chiral) ASI with in situ tunable array of chainlike magnetic charge order exhibits a high degree of electronic tunability, leading to multiple programmable superconducting properties and functionalities, such as switchable dissipationless/resistive states and reversible Hall effects. Furthermore, the vortex Hall effect signal can be not only reversed by flipping the polarity of the applied current but also inverted by changing the amplitude of the magnetic field. The vortex Hall effect can even be switched on/off by varying the ordering of the magnetic charges. In addition, the dynamical vortex behavior could be adjusted by tuning the angle between the direction of the driving current and the orientation of magnetic charge chains, which can be realized by rotating the orientation of the pinwheel ASI on the superconducting film. The performance of the hybrid device may further be improved by fine-tuning the parameters of the pinwheel ASI, such as the dimensions of the nanomagnets and the ASI lattice spacing, which would alter the interaction strength between the magnetic charges and superconducting vortices. This could lead to even more interesting phenomena and physics, such as reconfigurable dynamic vortex Mott transitions.[34] Finally, the method demonstrated here for tuning vortex motion using a pinwheel ASI could be applied to other topological charges such as magnetic skyrmions,[35] providing a universal and convenient approach to engineer new reprogrammable functionalities in magnetic particle systems. The reconfigurable magnetic potential landscape could also provide a perfect platform for tailoring spin−wave channels.[36]

## ■ ASSOCIATED CONTENT

### Supporting Information

The Supporting Information is available free of charge at https://pubs.acs.org/doi/10.1021/acs.nanolett.0c04093.

Videos S1−S4 showing results of MD simulations for vortex motion in sections A and B (at $B = 0.5B_0$ and $2B_0$) (MP4, MP4, MP4, MP4)

Calculation of vertex density and first matching field $B_0$, MD simulations of the distribution of vortices, and magnetic field and current dependences of the

Downloaded from pubs.acs.org/nalefd/article-pdf/20/12/8933/17691840/nl0c04093.pdf by NANJING UNIV user on 24 August 2026


https://dx.doi.org/10.1021/acs.nanolett.0c04093
Nano Lett. 2020, 20, 8933−8939

longitudinal voltages corresponding to the magnetic charge configurations shown in Figure 2c,d (PDF)

## AUTHOR INFORMATION


### Corresponding Authors

**Yong-Lei Wang** − *Research Institute of Superconductor Electronics, School of Electronic Science and Engineering, Nanjing University, Nanjing 210023, China;* orcid.org/0000-0003-0391-7757; Email: yongleiwang@nju.edu.cn

**Zhi-Li Xiao** − *Materials Science Division, Argonne National Laboratory, Argonne, Illinois 60439, United States; Department of Physics, Northern Illinois University, DeKalb, Illinois 60115, United States;* orcid.org/0000-0001-8012-2814; Email: xiao@anl.gov

**Huabing Wang** − *Research Institute of Superconductor Electronics, School of Electronic Science and Engineering, Nanjing University, Nanjing 210023, China; Purple Mountain Laboratories, Nanjing 211111, China;* orcid.org/0000-0003-4802-6077; Email: hbwang@nju.edu.cn

### Authors

**Yang-Yang Lyu** − *Research Institute of Superconductor Electronics, School of Electronic Science and Engineering, Nanjing University, Nanjing 210023, China; Materials Science Division, Argonne National Laboratory, Argonne, Illinois 60439, United States*

**Xiaoyu Ma** − *Department of Physics, University of Notre Dame, Notre Dame 46556, Indiana, United States*

**Jing Xu** − *Center for Nanoscale Materials, Argonne National Laboratory, Argonne, Illinois 60439, United States;* orcid.org/0000-0003-0160-7616

**Sining Dong** − *Research Institute of Superconductor Electronics, School of Electronic Science and Engineering, Nanjing University, Nanjing 210023, China*

**Boldizsar Janko** − *Department of Physics, University of Notre Dame, Notre Dame 46556, Indiana, United States*

**Ralu Divan** − *Center for Nanoscale Materials, Argonne National Laboratory, Argonne, Illinois 60439, United States*

**John E. Pearson** − *Materials Science Division, Argonne National Laboratory, Argonne, Illinois 60439, United States*

**Peiheng Wu** − *Research Institute of Superconductor Electronics, School of Electronic Science and Engineering, Nanjing University, Nanjing 210023, China*

**Wai-Kwong Kwok** − *Materials Science Division, Argonne National Laboratory, Argonne, Illinois 60439, United States*

Complete contact information is available at: https://pubs.acs.org/10.1021/acs.nanolett.0c04093


### Author Contributions

[+]Y.-Y.L. and X.M. contributed equally.

### Notes

The authors declare no competing financial interest.

## ACKNOWLEDGMENTS

This work is supported by the National Key R&D Program of China (2018YFA0209002), the National Natural Science Foundation of China (61771235, 61971464, 61727805, and 11961141002) and Jiangsu Shuangchuang Program. Magnetotransport measurements were supported by the U.S. Department of Energy, Office of Science, Basic Energy Sciences, Materials Sciences and Engineering. Use of the Center for Nanoscale Materials, an Office of Science user facility, was supported by the US Department of Energy, Office of Science, Office of Basic Energy Sciences, under contract number DE-AC02-06CH11357. J.X. and Z.-L.X. acknowledge support by the National Science Foundation under grant no. DMR-1901843.

## REFERENCES


(1) Abrikosov, A. A. On the Magnetic Properties of Superconductors of the Second Group. *J. Exp. Theor. Phys.* **1957**, *5*, 1174−1182.

(2) Gammel, P. Why Vortices Matter. *Nature* **2001**, *411*, 434−435.

(3) Savel'ev, S.; Nori, F. Experimentally Realizable Devices for Controlling the Motion of Magnetic Flux Quanta in Anisotropic Superconductors. *Nat. Mater.* **2002**, *1*, 179−184.

(4) Kwok, W. K.; Welp, U.; Glatz, A.; Koshelev, A. E.; Kihlstrom, K. J.; Crabtree, G. W. Vortices in High-Performance High-Temperature Superconductors. *Rep. Prog. Phys.* **2016**, *79*, 116501.

(5) Bugoslavsky, Y.; Cohen, L. F.; Perkins, G. K.; Polichetti, M.; Tate, T. J.; Gwilliam, R.; Caplin, A. D. Enhancement of the High-Magnetic-Field Critical Current Density of Superconducting $MgB_2$ by Proton Irradiation. *Nature* **2001**, *411*, 561−563.

(6) Díaz, A.; Mechin, L.; Berghuis, P.; Evetts, J. E. Evidence for Vortex Pinning by Dislocations in $YBa_2Cu_3O_{7-\delta}$ Low-Angle Grain Boundaries. *Phys. Rev. Lett.* **1998**, *80*, 3855−3858.

(7) Blatter, G.; Rhyner, J.; Vinokur, V. M. Vortex Pinning by Twin Boundaries in Copper Oxide Superconductors. *Phys. Rev. B: Condens. Matter Mater. Phys.* **1991**, *43*, 7826−7830.

(8) Tarantini, C.; Lee, S.; Zhang, Y.; Jiang, J.; Bark, C. W.; Weiss, J. D.; Polyanskii, A.; Nelson, C. T.; Jang, H. W.; Folkman, C. M.; Baek, S. H.; Pan, X. Q.; Gurevich, A.; Hellstrom, E. E.; Eom, C. B.; Larbalestier, D. C. Strong Vortex Pinning in Co-Doped $BaFe_2As_2$ Single Crystal Thin Films. *Appl. Phys. Lett.* **2010**, *96*, 142510.

(9) Llordés, A.; Palau, A.; Gázquez, J.; Coll, M.; Vlad, R.; Pomar, A.; Arbiol, J.; Guzmán, R.; Ye, S.; Rouco, V.; Sandiumenge, F.; Ricart, S.; Puig, T.; Varela, M.; Chateigner, D.; Vanacken, J.; Gutiérrez, J.; Moshchalkov, V.; Deutscher, G.; Magen, C.; Obradors, X. Nanoscale Strain-Induced Pair Suppression as a Vortex-Pinning Mechanism in High-Temperature Superconductors. *Nat. Mater.* **2012**, *11*, 329−336.

(10) Latimer, M. L.; Berdiyorov, G. R.; Xiao, Z. L.; Peeters, F. M.; Kwok, W. K. Realization of Artificial Ice Systems for Magnetic Vortices in a Superconducting MoGe Thin Film with Patterned Nanostructures. *Phys. Rev. Lett.* **2013**, *111*, 067001.

(11) Trastoy, J.; Malnou, M.; Ulysse, C.; Bernard, R.; Bergeal, N.; Faini, G.; Lesueur, J.; Briatico, J.; Villegas, J. E. Freezing and Thawing of Artificial Ice by Thermal Switching of Geometric Frustration in Magnetic Flux Lattices. *Nat. Nanotechnol.* **2014**, *9*, 710−715.

(12) Van Look, L.; Zhu, B. Y.; Jonckheere, R.; Zhao, B. R.; Zhao, Z. X.; Moshchalkov, V. V. Anisotropic Vortex Pinning in Superconductors with a Square Array of Rectangular Submicron Holes. *Phys. Rev. B: Condens. Matter Mater. Phys.* **2002**, *66*, 214511.

(13) Harada, K.; Kamimura, O.; Kasai, H.; Matsuda, T.; Tonomura, A.; Moshchalkov, V. V. Direct Observation of Vortex Dynamics in Superconducting Films with Regular Arrays of Defects. *Science* **1996**, *274*, 1167−1170.

(14) Wang, Y. L.; Latimer, M. L.; Xiao, Z. L.; Divan, R.; Ocola, L. E.; Crabtree, G. W.; Kwok, W. K. Enhancing the Critical Current of a Superconducting Film in a Wide Range of Magnetic Fields with a Conformal Array of Nanoscale Holes. *Phys. Rev. B: Condens. Matter Mater. Phys.* **2013**, *87*, 220501.

(15) Patel, U.; Xiao, Z. L.; Hua, J.; Xu, T.; Rosenmann, D.; Novosad, V.; Pearson, J.; Welp, U.; Kwok, W. K.; Crabtree, G. W. Origin of the Matching Effect in a Superconducting Film with a Hole Array. *Phys. Rev. B: Condens. Matter Mater. Phys.* **2007**, *76*, 020508.

(16) Latimer, M. L.; Berdiyorov, G. R.; Xiao, Z. L.; Kwok, W. K.; Peeters, F. M. Vortex Interaction Enhanced Saturation Number and Caging Effect in a Superconducting Film with a Honeycomb Array of Nanoscale Holes. *Phys. Rev. B: Condens. Matter Mater. Phys.* **2012**, *85*, 012515.


Downloaded from pubs.acs.org/nalefd/article-pdf/20/12/8933/17691840/nl0c04093.pdf by NANJING UNIV user on 24 August 2026

(17) Villegas, J. E.; Savel'ev, S.; Nori, F.; Gonzalez, E. M.; Anguita, J. V.; García, R.; Vicent, J. L. A Superconducting Reversible Rectifier That Controls the Motion of Magnetic Flux Quanta. *Science* **2003**, *302*, 1188−1191.
(18) Martín, J. I.; Vélez, M.; Hoffmann, A.; Schuller, I. K.; Vicent, J. L. Artificially Induced Reconfiguration of the Vortex Lattice by Arrays of Magnetic Dots. *Phys. Rev. Lett.* **1999**, *83*, 1022.
(19) Silhanek, A. V.; Gillijns, W.; Moshchalkov, V. V.; Zhu, B. Y.; Moonens, J.; Leunissen, L. H. A. Enhanced Pinning and Proliferation of Matching Effects in a Superconducting Film with a Penrose Array of Magnetic Dots. *Appl. Phys. Lett.* **2006**, *89*, 152507.
(20) Morgan, D. J.; Ketterson, J. B. Asymmetric Flux Pinning in a Regular Array of Magnetic Dipoles. *Phys. Rev. Lett.* **1998**, *80*, 3614−3617.
(21) Martín, J. I.; Vélez, M.; Nogués, J.; Schuller, I. K. Flux Pinning in a Superconductor by an Array of Submicrometer Magnetic Dots. *Phys. Rev. Lett.* **1997**, *79*, 1929−1932.
(22) Kramer, R. B. G.; Silhanek, A. V.; Van De Vondel, J.; Raes, B.; Moshchalkov, V. V. Symmetry-Induced Giant Vortex State in a Superconducting Pb Film with a Fivefold Penrose Array of Magnetic Pinning Centers. *Phys. Rev. Lett.* **2009**, *103*, 067007.
(23) Silhanek, A. V.; Gillijns, W.; Moshchalkov, V. V.; Metlushko, V.; Ilic, B. Tunable Pinning in Superconducting Films with Magnetic Microloops. *Appl. Phys. Lett.* **2006**, *89*, 182505.
(24) Lange, M.; Bael, M. J. V.; Bruynseraede, Y.; Moshchalkov, V. V. Nanoengineered Magnetic-Field-Induced Superconductivity. *Phys. Rev. Lett.* **2003**, *90*, 197006.
(25) Gomez, A.; Gilbert, D. A.; Gonzalez, E. M.; Liu, K.; Vicent, J. L. Control of Dissipation in Superconducting Films by Magnetic Stray Fields. *Appl. Phys. Lett.* **2013**, *102*, 052601.
(26) Perez De Lara, D.; Castaño, F. J.; Ng, B. G.; Körner, H. S.; Dumas, R. K.; Gonzalez, E. M.; Liu, K.; Ross, C. A.; Schuller, I. K.; Vicent, J. L. Magnetic Pinning of Flux Lattice in Superconducting-Nanomagnet Hybrids. *Appl. Phys. Lett.* **2011**, *99*, 182509.
(27) De Souza Silva, C. C.; Silhanek, A. V.; Van De Vondel, J.; Gillijns, W.; Metlushko, V.; Ilic, B.; Moshchalkov, V. V. Dipole-Induced Vortex Ratchets in Superconducting Films with Arrays of Micromagnets. *Phys. Rev. Lett.* **2007**, *98*, 117005.
(28) Rollano, V.; Muñoz-Noval, A.; Gomez, A.; Valdes-Bango, F.; Martin, J. I.; Velez, M.; Osorio, M. R.; Granados, D.; Gonzalez, E. M.; Vicent, J. L. Topologically Protected Superconducting Ratchet Effect Generated by Spin-Ice Nanomagnets. *Nanotechnology* **2019**, *30*, 244003.
(29) Wang, Y. L.; Ma, X.; Xu, J.; Xiao, Z. L.; Snezhko, A.; Divan, R.; Ocola, L. E.; Pearson, J. E.; Janko, B.; Kwok, W. K. Switchable Geometric Frustration in an Artificial-Spin-Ice-Superconductor Heterosystem. *Nat. Nanotechnol.* **2018**, *13*, 560−565.
(30) Wang, R. F.; Nisoli, C.; Freitas, R. S.; Li, J.; McConville, W.; Cooley, B. J.; Lund, M. S.; Samarth, N.; Leighton, C.; Crespi, V. H.; Schiffer, P. Artificial "spin Ice" in a Geometrically Frustrated Lattice of Nanoscale Ferromagnetic Islands. *Nature* **2006**, *439*, 303−306.
(31) Skjærvø, S. H.; Marrows, C. H.; Stamps, R. L.; Heyderman, L. J. Advances in Artificial Spin Ice. *Nat. Rev. Phys.* **2020**, *2*, 13−28.
(32) Gliga, S.; Hrkac, G.; Donnelly, C.; Büchi, J.; Kleibert, A.; Cui, J.; Farhan, A.; Kirk, E.; Chopdekar, R. V.; Masaki, Y.; Bingham, N. S.; Scholl, A.; Stamps, R. L.; Heyderman, L. J. Emergent Dynamic Chirality in a Thermally Driven Artificial Spin Ratchet. *Nat. Mater.* **2017**, *16*, 1106−1111.
(33) Li, Y.; Paterson, G. W.; Macauley, G. M.; Nascimento, F. S.; Ferguson, C.; Morley, S. A.; Rosamond, M. C.; Linfield, E. H.; Maclaren, D. A.; Macêdo, R.; et al. Superferromagnetism and Domain-Wall Topologies in Artificial "Pinwheel" Spin Ice. *ACS Nano* **2019**, *13*, 2213−2222.
(34) Poccia, N.; Baturina, T. I.; Coneri, F.; Molenaar, C. G.; Wang, X. R.; Bianconi, G.; Brinkman, A.; Hilgenkamp, H.; Golubov, A. A.; Vinokur, V. M. Critical Behavior at a dynamic vortex insulator-to-metal transition. *Science* **2015**, *349*, 1202−1205.
(35) Ma, X.; Reichhardt, C. J. O.; Reichhardt, C. Reversible Vector Ratchets for Skyrmion Systems. *Phys. Rev. B: Condens. Matter Mater. Phys.* **2017**, *95*, 104401.
(36) Iacocca, E.; Gliga, S.; Heinonen, O. G. Tailoring Spin-Wave Channels in a Reconfigurable Artificial Spin Ice. *Phys. Rev. Appl.* **2020**, *13*, 044047.

Downloaded from pubs.acs.org/nalefd/article-pdf/20/12/8933/17691840/nl0c04093.pdf by NANJING UNIV user on 24 August 2026


https://dx.doi.org/10.1021/acs.nanolett.0c04093
*Nano Lett.* 2020, 20, 8933−8939